SUPPORTING INFORMATION

Water Quality Prediction of Small-Micro Water Body Based on The Intelligent-Algorithm-Optimized Support Vector Machine Regression Method and Unmanned Aerial Vehicles Multispectral Data

Ke Yao [1], Yujie Chen [1], Yucheng Li [1,*], Xuesheng Zhang [1], Beibei Zhu [1], Zihao Gao [1], Fei Lin [2,3,*] and Yimin Hu [2,3]

[1] School of Resources and Environmental Engineering, Anhui University, Hefei 230601, China; yaoke1031@163.com (K.Y.); 17856419489@163.com (Y.C.); zhangqing8725@163.com (X.Z.); 18305508976@163.com (B.Z.); gzh195423@163.com (Z.G.)
[2] Hefei Intelligent Agriculture Collaborative Innovation Research Institute, Hefei 230031, China; ymhu@iim.ac.cn
[3] Institute of Intelligent Machines, Hefei Institutes of Physical Science, Chinese Academy of Sciences, Hefei 230031, China
* Correspondence: li-yucheng@163.com (Y.L.); feilin@iim.ac.cn (F.L.)

Tables

Table S1. Water quality parameter detection method.

Water quality parameters	Detection method
Chla	Spectrophotometry (HJ 897-2017)
TP	Ammonium molybdate spectrophotometry (GB 11893-89)
NH_3-N	Nessler's reagent spectrophotometric method (HJ 535-2009)
TUB	Field instrument measurement (turbidimeter (2100Q01-CN, HACH, Shanghai, China))

Figure legends

Figure S1. Comparison of the accuracy of basic-SVR and optimized-SVR models for TP.	S-3
Figure S2. The scatter plots of predicted values and measured values of TP using different SVR models:(a) GWO-SVR;(b) GA-SVR;(c) PSO-SVR;(d) SVR;(e) ACO-SVR;(f) FA-SVR;(g) HPO-SVR.	S-4
Figure S3. Comparison of prediction performance of eight SVR models for NH_3-N.	S-5
Figure S4. The fitting graph of the measured and predicted values of NH_3-N: (a) GWO-SVR; (b) GA-SVR; (c) PSO-SVR; (d) SVR; (e) ACO-SVR; (f) FA-SVR; (g) HPO-SVR.	S-6
Figure S5. Comparison of prediction performance of eight SVR models for TUB.	S-7
Figure S6. The fitting graph of the measured and predicted values of TUB :(a) GWO-SVR;(b) GA-SVR;(c) PSO-SVR;(d) SVR;(e) ACO-SVR;(f) FA-SVR;(g) HPO-SVR.	S-8

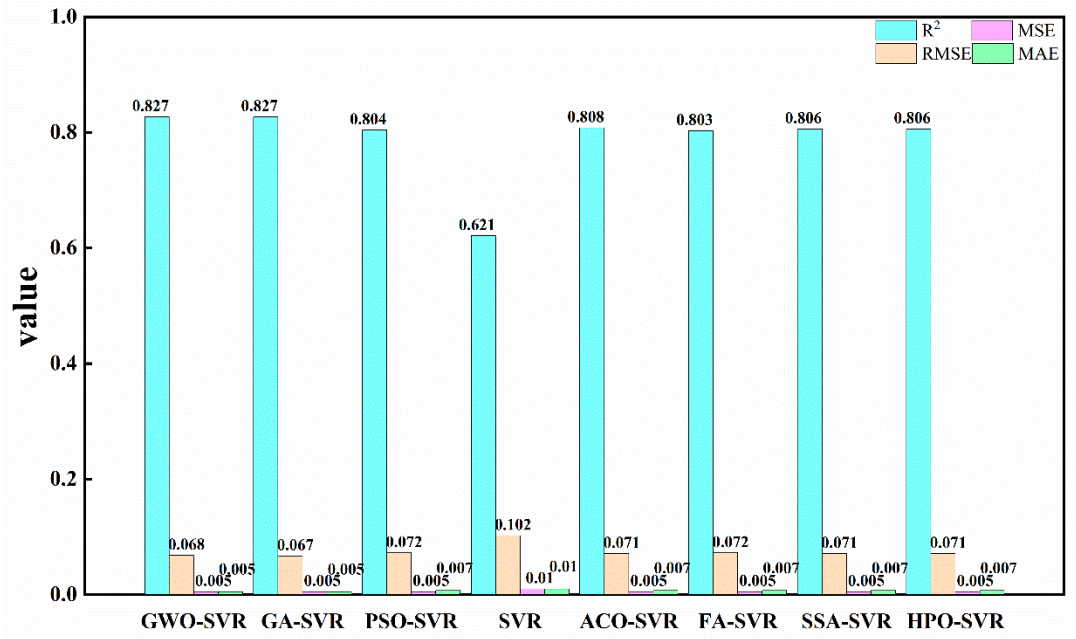


Figure S1. Comparison of the accuracy of basic-SVR and optimized-SVR models for TP.

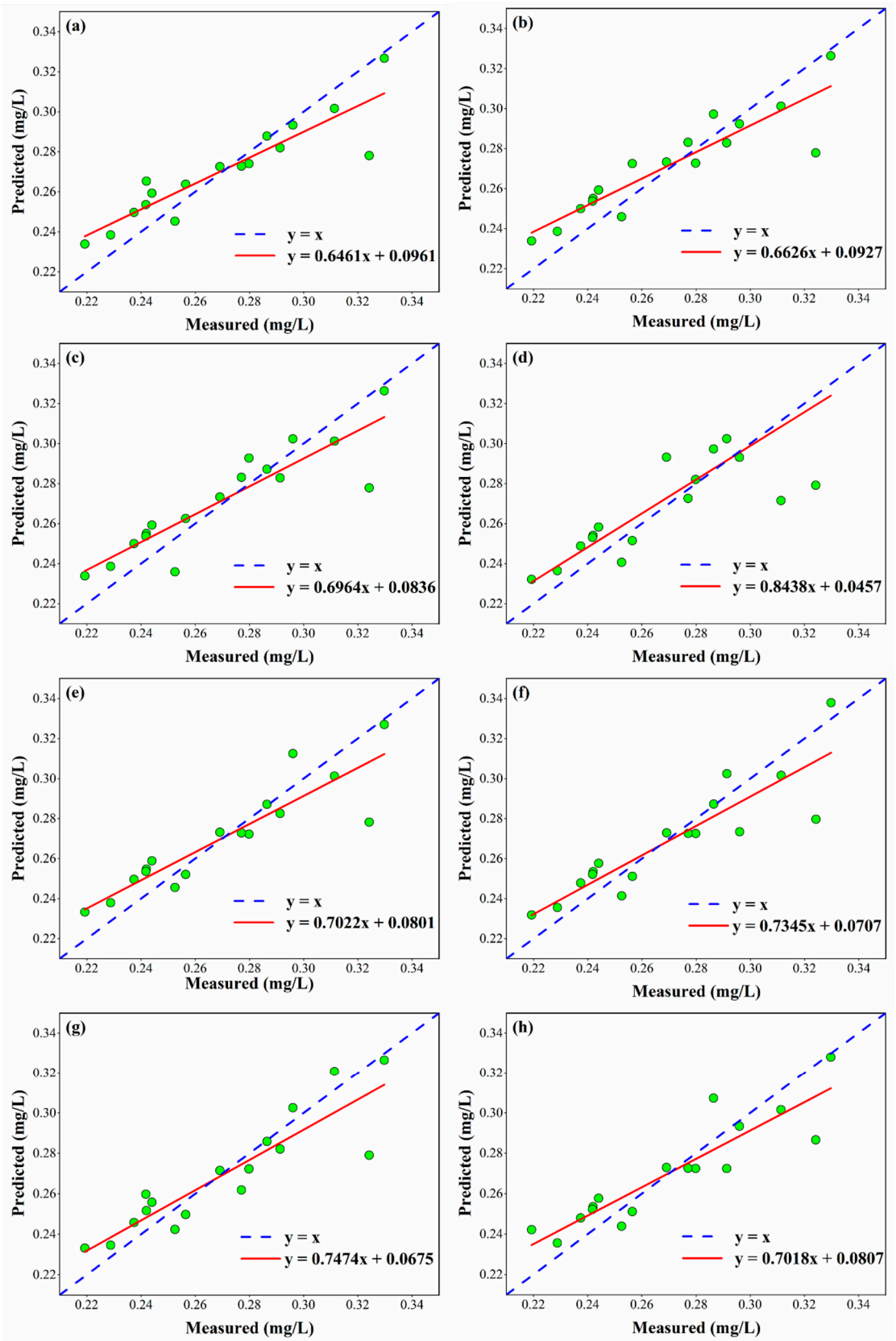


Figure S2. The scatter plots of predicted values and measured values of TP using different SVR models:(a) GWO-SVR;(b) GA-SVR;(c) PSO-SVR;(d) SVR;(e) ACO-SVR;(f) FA-SVR;(g) HPO-SVR.

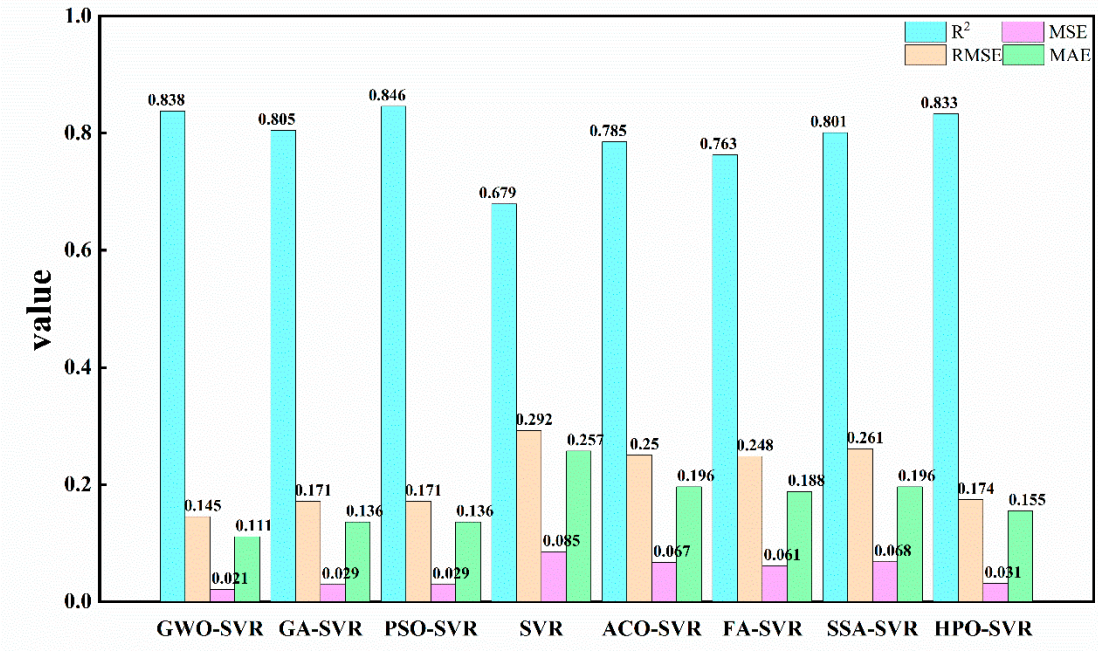


Figure S3. Comparison of prediction performance of eight SVR models for NH_3-N.

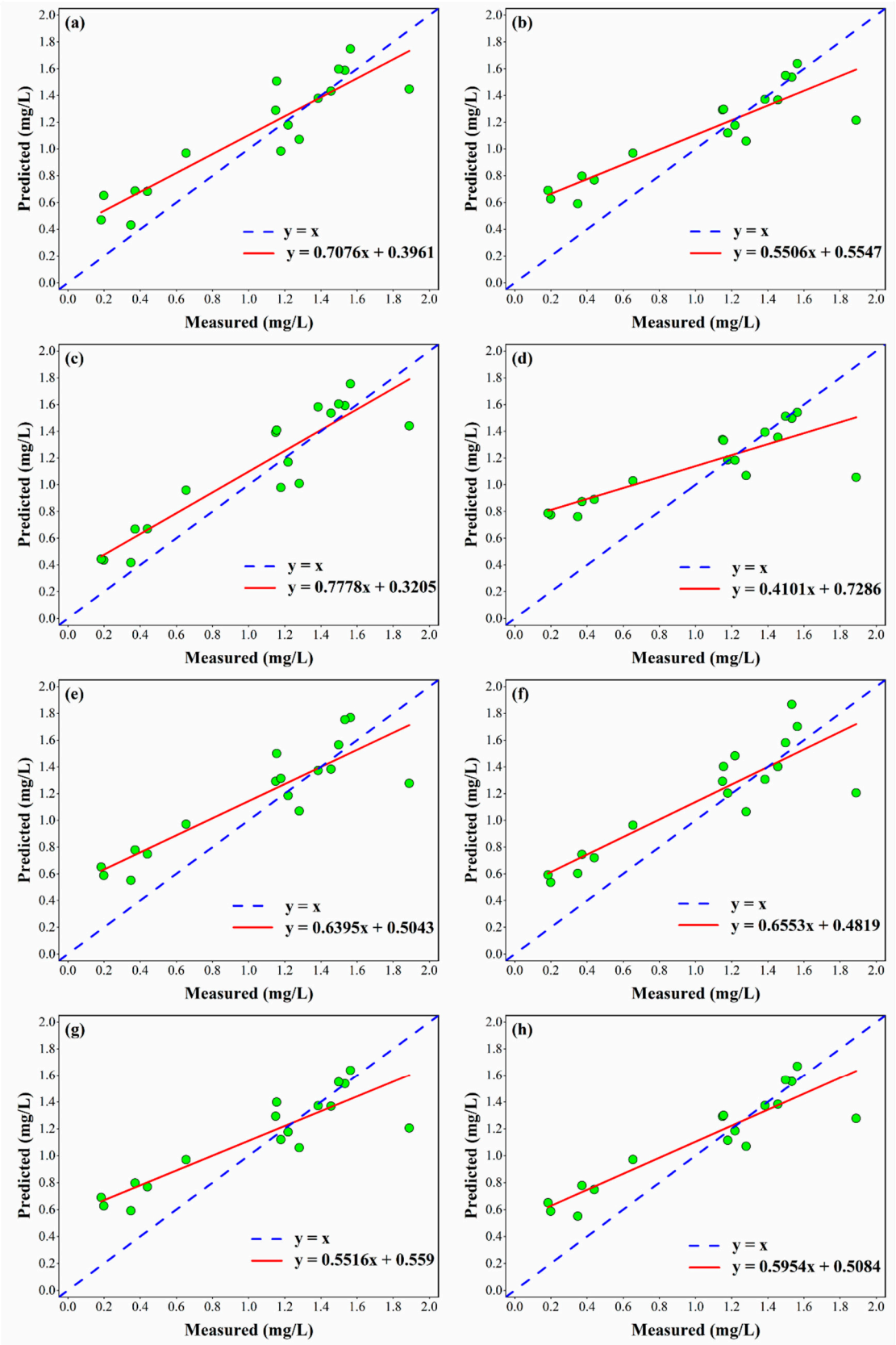


Figure S4. The fitting graph of the measured and predicted values of NH_3-N: (a) GWO-SVR; (b) GA-SVR; (c) PSO-SVR; (d) SVR; (e) ACO-SVR; (f) FA-SVR; (g) HPO-SVR.

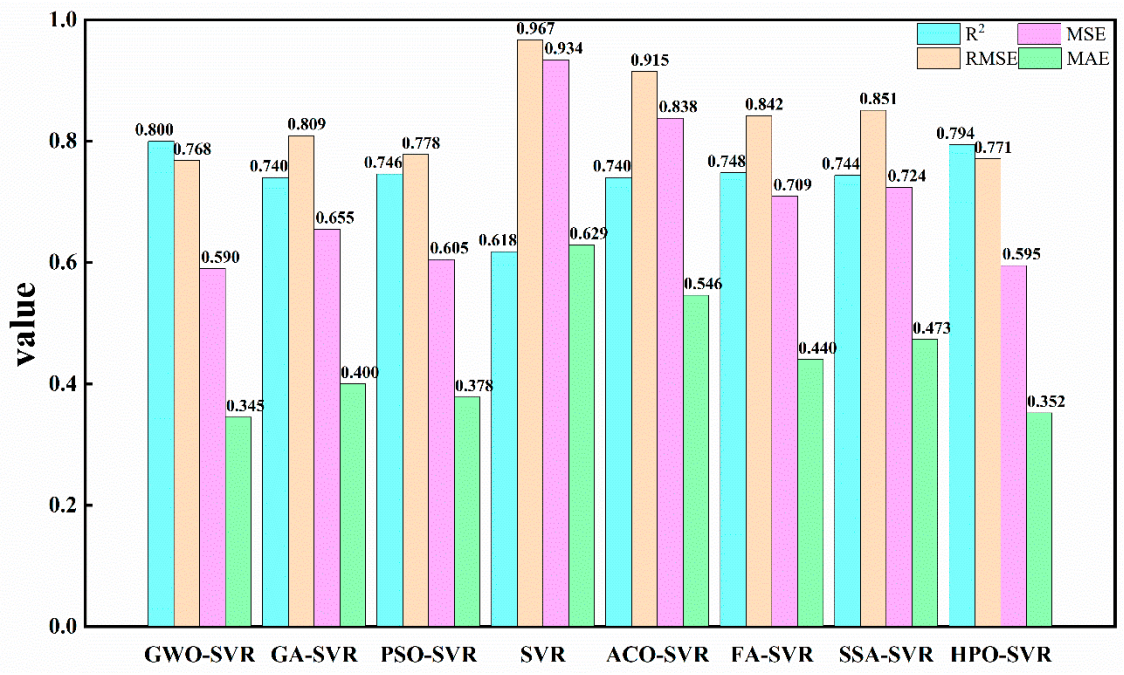


Figure S5. Comparison of prediction performance of eight SVR models for TUB.

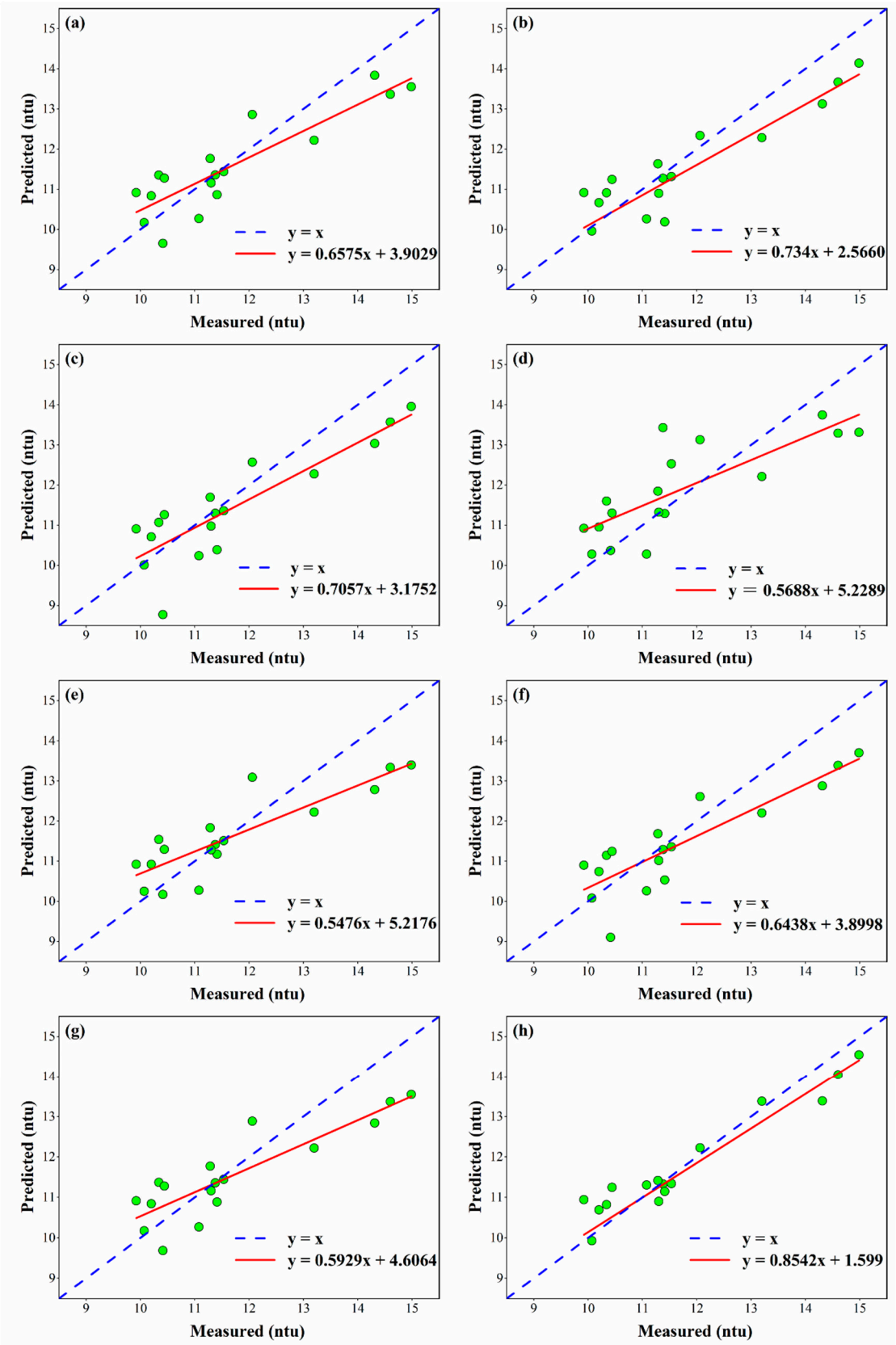


Figure S6. The fitting graph of the measured and predicted values of TUB :(a) GWO-SVR;(b) GA-SVR;(c) PSO-SVR;(d) SVR;(e) ACO-SVR;(f) FA-SVR;(g) HPO-SVR.